A Novel Na(I) Coordination Complex with s-Triazine Pincer Ligand: Synthesis, X-ray Structure, Hirshfeld Analysis, and Antimicrobial Activity

crystals

MDPI

Article

A Novel Na(I) Coordination Complex with *s*-Triazine Pincer Ligand: Synthesis, X-ray Structure, Hirshfeld Analysis, and Antimicrobial Activity

Amal Yousri [1,*], Ayman El-Faham [1], Matti Haukka [2], Mohammed Salah Ayoup [1], Magda M. F. Ismail [3], Nagwan G. El Menofy [4], Saied M. Soliman [1,*], Lars Öhrström [5], Assem Barakat [6] and Morsy A. M. Abu-Youssef [1,*]

1 Department of Chemistry, Faculty of Science, Alexandria University, Ibrahimia, P.O. Box 426, Alexandria 21321, Egypt; ayman.elfaham@alexu.edu.eg or aymanel_faham@hotmail.com (A.E.-F.); mohamed.salah@alexu.edu.eg (M.S.A.)
2 Department of Chemistry, University of Jyväskylä, P.O. Box 35, FI-40014 Jyväskylä, Finland; matti.o.haukka@jyu.fi
3 Department of Pharmaceutical Medicinal Chemistry, Faculty of Pharmacy (Girls), Al-Azhar University, Cairo 11754, Egypt; magdaismail@azhar.edu.eg or m.elalfy101@gmail.com
4 Department of Microbiology and Immunology, Faculty of Pharmacy (Girls), Al-Azhar University, Cairo 11754, Egypt; nagwan.elmenofy@azhar.edu.eg
5 Department of Chemistry and Chemical Engineering, Chalmers University of Technology, SE-41296 Gothenburg, Sweden; ohrstrom@chalmers.se
6 Department of Chemistry, College of Science, King Saud University, P.O. Box 2455, Riyadh 11451, Saudi Arabia; ambarakat@ksu.edu.sa
* Correspondence: amal.yousri@alexu.edu.eg or amalyousri@yahoo.com (A.Y.); saied1soliman@yahoo.com (S.M.S.); morsy5@alexu.edu.eg (M.A.M.A.-Y.)

check for updates

Citation: Yousri, A.; El-Faham, A.; Haukka, M.; Ayoup, M.S.; Ismail, M.M.F.; Menofy, N.G.E.; Soliman, S.M.; Öhrström, L.; Barakat, A.; Abu-Youssef, M.A.M. A Novel Na(I) Coordination Complex with *s*-Triazine Pincer Ligand: Synthesis, X-ray Structure, Hirshfeld Analysis, and Antimicrobial Activity. *Crystals* **2023**, *13*, 890. https://doi.org/10.3390/cryst13060890

Academic Editor: Kil Sik Min

Received: 5 May 2023
Revised: 19 May 2023
Accepted: 25 May 2023
Published: 29 May 2023

Abstract: The pincer ligand 2,4-*bis*(3,5-dimethyl-1*H*-pyrazol-1-yl)-6-methoxy-1,3,5-triazine (**bpmt**) was used to synthesize the novel $[Na(bpmt)_2][AuCl_4]$ complex through the self-assembly method. In this complex, the Na(I) ion is hexa-coordinated with two tridentate *N*-pincer ligands (**bpmt**). The two **bpmt** ligand units are meridionally coordinated to Na(I) via one short $Na\text{-}N_{(s\text{-triazine})}$ and two slightly longer $Na\text{-}N_{(pyrazole)}$ bonds, resulting in a distorted octahedral geometry around the Na(I) ion. In the coordinated **bpmt** ligand, the *s*-triazine core is not found to be coplanar with the two pyrazole moieties. Additionally, the two **bpmt** units are strongly twisted from one another by 64.94°. Based on Hirshfeld investigations, the H···H (53.4%) interactions have a significant role in controlling the supramolecular arrangement of the $[Na(bpmt)_2][AuCl_4]$ complex. In addition, the Cl···H (12.2%), C···H (11.5%), N···H (9.3%), and O···H (4.9%) interactions are significant. Antimicrobial investigations revealed that the $[Na(bpmt)_2][AuCl_4]$ complex has promising antibacterial and antifungal activities. The $[Na(bpmt)_2][AuCl_4]$ complex showed enhanced antibacterial activity for the majority of the studied gram-positive and gram-negative bacteria compared to the free **bpmt** (MIC = 62.5–125 μg/mL vs. MIC = 62.5–500 μg/mL, respectively) and Amoxicillin (MIC > 500 μg/mL) as a positive control. Additionally, the $[Na(bpmt)_2][AuCl_4]$ complex had better antifungal efficacy (MIC = 125 μg/mL) against *C. albicans* compared to **bpmt** (MIC = 500 μg/mL).

Keywords: Na(I) coordination complex; *s*-triazine pincer ligand; X-ray; Hirshfeld surface; antimicrobial activity

1. Introduction

One of the most important pharmaceutical concerns in medicine is antibiotic-resistant microorganisms [1,2]. Efforts to address the serious problems arising from microbial infections include the design of novel antimicrobial agents with minimal side effects and enhanced chemical and pharmacological characteristics [3,4]. Generally, metal ions play a

crucial role in biological processes due to their interactions with numerous biomolecules, including amino acids, enzymes, and serum albumin [5–7]. Thus, the self-assembly of individual molecules via non-covalent interactions, particularly metal–organic complexes, is one of the most promising research areas in this field [8–12]. The need to create molecular structures that can mimic the naturally existing molecules has driven researchers' interest in the coordination chemistry of alkali metal ions in recent decades. The best example of alkali metal ions is Na(I), which is necessary for biological systems [13] and plays a crucial role in cancer therapy as it can make tumor cells more susceptible to death [14–18]. Recently, many Na(I) complexes have been reported and analyzed to determine their supramolecular structures [19–22]. It has been found that Na(I) can form homodinuclear, heterodinuclear, and trimetallic complexes [23–26]. Additionally, Na(I) can create coordination complexes with unexpected coordination geometries and various coordination numbers (CN). The coordination geometry of Na(I) can be tetrahedral (CN = 4), trigonal bipyramidal (CN = 5), octahedral (CN = 6), pentagonal pyramidal (CN = 7), square antiprism (CN = 8), dodecahedral (CN = 8), and trigonal-dodecahedral (CN = 8) [27–31].

In the literature, sodium complexes with octahedral coordination geometry are well known. For example, a 2D polymeric sodium complex with *bis*-tetrazole type ligand was reported by Sobral et. al. In this complex, the sodium metal ion has a distorted octahedral environment with a $NaNO_5$ coordination sphere [32]. Another example is the mononuclear octahedral [Prolinate$_2$-Na(MeOH)$_4$]$^-$H$^+$ complex, which has a NaO_6 coordination sphere [33]. In this case, the sodium ion is coordinated with four methanol molecules and two prolinate anions as monodentate ligands. Furthermore, a new distorted octahedral sodium complex, [Na(H_2O)$_5$(DMF)]·(L) (L=1,5-naphthalenedisulfonate), was obtained, and its single crystal structure confirmed the NaO_6 coordination sphere via one DMF and five H_2O molecules [22]. A hepta-coordinated sodium complex was reported by Gourdon's research group with dipicolinic acid as a ligand, and its structure was confirmed using single crystal X-ray structure, also showing a $NaNO_6$ coordination environment [34]. To the best of our knowledge, there are no well-known pincer sodium complexes with *s*-triazine N-donor ligands and confirmed structures. However, Beer et al. reported a new sodium complex with *bis*-triazacyclononane *tris*-pyridyl N9-azacryptand as ligand [35]. This is considered the only pincer sodium complex that has been structurally characterized using single crystal X-ray crystallography (SCXRD) with nitrogen macrocyclic ligands, and it exhibits a NaN_9 coordination environment. The most frequent ligands that form coordination compounds with alkali metal ions are Schiff bases, tridentate ligands (such as *o*-vanillin and benzhydryl ligands), crown ethers, etc. [23,36–38]. Generally, multidentate ligands play a significant role in coordination chemistry as they can form extra-stable metal complexes due to the chelate effect. Among these multidentate ligands, symmetrical triazine (*s*-triazine) derivatives are promising due to their diverse biological effects and powerful pharmacological properties [39–43]. Moreover, substances containing pyrazoles are considered effective biological agents [44–46]. Among *s*-triazine derivatives, the 2,4-*bis*(3,5-dimethyl-1*H*-pyrazol-1-yl)-6-methoxy-1,3,5-triazine (**bpmt**) ligand has been extensively studied by our research team for many reasons [4,47–57]. The **bpmt** ligand can be easily prepared with a high yield, and it is classified as a tridentate *N*-pincer ligand with different coordination behaviors. In addition, its metal complexes exhibit remarkable biological activities compared to the free **bpmt** ligand [4,48,51–53,55,56,58]. The pincer complexes of **bpmt** are stable and can be simply synthesized via the self-assembly of the functional ligand (**bpmt**) with a metal salt [54,57].

The goal of the current work was to synthesize a new pincer complex of the **bpmt** ligand through self-assembly with Na[$AuCl_4$].2H_2O. The molecular and supramolecular structures of the complex were explored using single crystal X-ray diffraction in combination with Hirshfeld calculations. In addition, the antimicrobial activity of the complex was evaluated.

2. Materials and Methods

2.1. Chemicals and Instrumentations

All chemicals were obtained from Sigma-Aldrich Company. Perkin-Elmer 2400 equipment (PerkinElmer, Waltham, MA, USA) was used to perform the elemental analyses (CHN). The FTIR spectra in KBr pellets were recorded in the range 4000–400 cm^{-1} using a Bruker Tensor 37 instrument (Waltham, MA, USA). NMR spectra were recorded in DMSO-d_6 as a solvent using a JEOL-400 MHz spectrometer (JEOL, Ltd., Tokyo, Japan) at 298 K. Na content was determined using a Shimadzu atomic absorption spectrophotometer (AA-7000 series, Shimadzu, Ltd., Tokyo, Japan).

2.2. Syntheses

The **bpmt** pincer ligand was prepared using the procedure previously reported by our research group [57,59].

Synthesis of the $[Na(bpmt)_2][AuCl_4]$ Complex

A 10 mL ethanolic solution of $Na[AuCl_4]\cdot 2H_2O$ (39.8 mg, 0.1 mmol) was mixed with 10 mL of a hot ethanolic solution of **bpmt** (59.8 mg, 0.2 mmol). The resulting clear mixture was left at room-temperature for slow evaporation. After three days, yellow crystals were formed, which were collected through filtration and found suitable for single crystal X-ray diffraction measurements.

The yield of the reaction was 89%. The analytical calculation for $C_{28}H_{34}AuCl_4N_{14}NaO_2$ yielded the following percentages: C, 35.02; H, 3.57; N, 20.42; Na, 22.99%. Upon analysis, the found percentages were as follows: C, 35.19; H, 3.45; N, 20.28%; Na, 22.78%.

The FTIR spectra of $[Na(bpmt)_2][AuCl_4]$ exhibited peaks at the following wavenumbers (cm^{-1}): 3421, 3107, 2956, 2930, 1601, 1548, 1417, 1367, 1221, 1123, 1046, 971, 813, and 750 (Figure S1, Supplementary Data). The FTIR spectra of the ligand (**bpmt**) displayed peaks at the following wavenumbers (cm^{-1}): 3392, 3313, 2986, 2930, 1597, 1558, 1408, 1373, 1224, 1128, 1041, 973, 812, and 751 (Figure S2, Supplementary Data). The ^{1}H NMR spectrum of $[Na(bpmt)_2][AuCl_4]$ (500 MHz, DMSO-d_6) revealed the following chemical shifts: δ_H 6.23 (s, 2H, Ar-H), 4.02 (s, 3H, OCH_3), 2.64 (s, 6H, $2CH_3$), 2.19 (s, 6H, $2CH_3$) ppm. The ^{13}C NMR spectrum (125 MHz, DMSO-d_6) displayed the following chemical shifts: δ_C 172.4, 164.8, 152.6, 144.7, 112.2, 56.3, 15.9, 14.1 ppm (Figure S3, Supplementary Data).

The ^{1}H NMR spectrum of the ligand (**bpmt**) (500 MHz, DMSO-d_6) exhibited the following chemical shifts: δ_H 6.22 (s, 2H, Ar-H), 4.01 (s, 3H, OCH_3), 2.64 (s, 6H, $2CH_3$), and 2.16 (s, 6H, $2CH_3$) ppm. The ^{13}C NMR spectrum (125 MHz, DMSO-d_6) displayed the following chemical shifts: δ_C 172.3, 164.8, 152.4, 144.6, 112.2, 56.3, 15.9, and 14.1 ppm (Figure S4, Supplementary Data).

2.3. Crystal Structure Determination

The crystal of $[Na(bpmt)_2][AuCl_4]$ was immersed in cryo-oil, mounted in a loop, and measured at a temperature of 170 K. The X-ray diffraction data were collected using a Bruker Kappa Apex II diffractometer with Mo Kα radiation. The *Denzo-Scalepack* [60] software package was used for cell refinement and data reduction. A multi-scan absorption correction based on equivalent reflections (*SADABS* [61]) was applied to the intensities before the structure solution. The structure was solved using the intrinsic phasing method with *SHELXT* [62] software. Structural refinement was carried out using *SHELXL* [63] software with the *SHELXLE* [64] graphical user interface. All the hydrogen atoms were positioned geometrically and constrained to ride on their parent atoms, with C-H = 0.95–0.98 Å and U_{iso} = 1.2–1.5 U_{eq} (parent atom). The crystal data and structure refinement details are shown in Table 1.

Table 1. Crystal data for $[Na(bpmt)_2][AuCl_4]$.

CCDC	2252757
empirical formula	$C_{28}H_{34}AuCl_4N_{14}NaO_2$
fw	960.45
temp (K)	170(2)
λ(Å)	0.71073
cryst syst	Monoclinic
space group	$P2_1/c$
a (Å)	10.24060(10)
b (Å)	14.12690(10)
c (Å)	26.0992(3)
β (deg)	96.2770(10)
V (Å^3)	3753.08(6)
Z	4
ρ_{calc} (Mg/m^3)	1.700
μ(Mo Kα) (mm^{-1})	4.264
No. reflns.	63394
Unique reflns.	9264
Completeness to θ = 25.242°	99.2%
GOOF (F^2)	1.038
R_{int}	0.0365
$R1$ [a] ($I \geq 2\sigma$)	0.0335
$wR2$ [b] ($I \geq 2\sigma$)	0.644

[a] $R1 = \Sigma||F_o| - |F_c||/\Sigma|F_o|$. [b] $wR2 = \{\Sigma[w(F_o^2 - F_c^2)^2]/\Sigma[w(F_o^2)^2]\}^{1/2}$.

2.4. Hirshfeld Surface Analysis

The topology analyses were performed using the Crystal Explorer 17.5 program [65] to generate 2D fingerprint plots and Hirshfeld surfaces [66].

2.5. Antimicrobial Studies

The antimicrobial activity [67] of the investigated ligand and its Na(I) complex were determined, as described in Method S1 (Supplementary Data).

3. Results and Discussion

3.1. Synthesis and Characterizations

The novel $[Na(bpmt)_2][AuCl_4]$ complex was synthesized using a self-assembly technique by reacting $Na[AuCl_4].2H_2O$ with the **bpmt** ligand (Scheme 1). Several spectroscopic techniques were used to confirm the structure of the resulting complex. Figures S1 and S2 (Supplementary Data) show the FTIR spectra of the $[Na(bpmt)_2][AuCl_4]$ complex compared to the free **bpmt** ligand. The FTIR spectra of the $[Na(bpmt)_2][AuCl_4]$ complex revealed the main vibrational characteristics of the functional organic ligand (**bpmt**) with slight variations. The stretching modes $\upsilon_{(C=N)}$ and $\upsilon_{(C=C)}$ in the free **bpmt** appeared at 1597 and 1558 cm^{-1}, respectively. In the $[Na(bpmt)_2][AuCl_4]$ complex, these stretching modes were observed at 1601 and 1548 cm^{-1}, respectively. It was observed that the coordination of Na(I) with **bpmt** resulted in a blue shift for the $\upsilon_{(C=N)}$ mode and a red shift in the $\upsilon_{(C=C)}$ mode [55,57]. Thus, the complexation had an impact on both vibrational bands compared with the free ligand. Moreover, single crystal X-ray diffraction combined with Hirshfeld surface analysis was used to specifically determine the molecular and supramolecular structures of the $[Na(bpmt)_2][AuCl_4]$ complex.

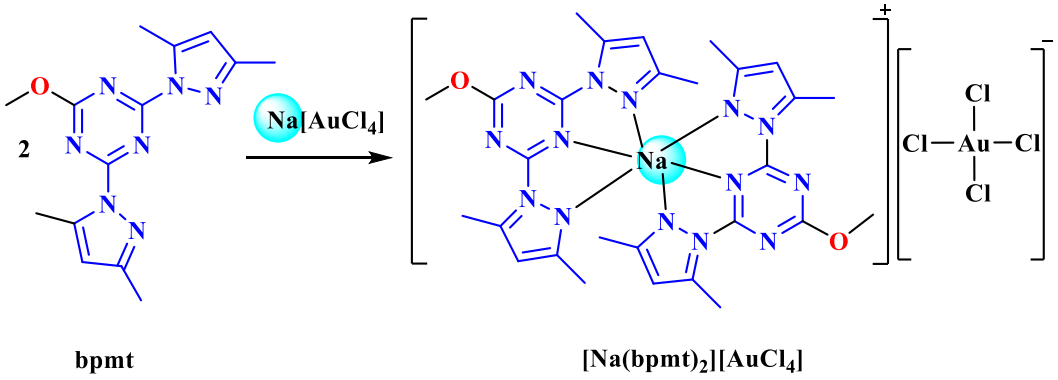

Scheme 1. Synthesis of the $[Na(bpmt)_2][AuCl_4]$ complex.

3.2. Crystal Structure Description

The X-ray structure of the $[Na(bpmt)_2][AuCl_4]$ complex unequivocally confirmed the coordination between Na(I) and the **bpmt** ligand. The asymmetric unit of the resulting complex is shown in Figure 1, consisting of one formula unit of the cationic complex $[Na(bpmt)_2][AuCl_4]$. In this complex, the Na(I) ion coordinates with two units of the pincer ligand **bpmt** via the N-atoms of the two pyrazolyl moieties and one N-atom from the *s*-triazine core, while the tetrachloroaurate serves as the counter anion. The Na-N bond distances with the *s*-triazine core were found to be 2.443(3) Å (Na1-N5) and 2.429(3) Å (Na1-N12). It is worth noting that the two *s*-triazine cores of the two **bpmt** ligand units were found to be coordinated with the Na(I) ion in a trans configuration. The N5-Na-N12 angle was found to be 171.65(10)°, which was slightly deviated from the ideal value of 180°. Hence, the two **bpmt** ligand units were meridionally coordinated to the Na(I) ion. The Na-N bonds with the pyrazolyl moieties are generally slightly longer (2.438(3)–2.538(3) Å) than the $Na\text{-}N_{(s\text{-triazine})}$ bond. The bite angles of the **bpmt** pincer chelate were in the range of 63.96(9)–64.98(9)°. In addition, the trans $N_{(pyrazole)}\text{-}Na\text{-}N_{(pyrazole)}$ angles significantly deviated from the ideal value of 180°. The N(1)-Na(1)-N(7) and N(8)-Na(1)-N(14) angles were determined to be 128.40(9) and 128.18(9)°, respectively. The Na-N and N-Na-N angles are listed in Table 2.

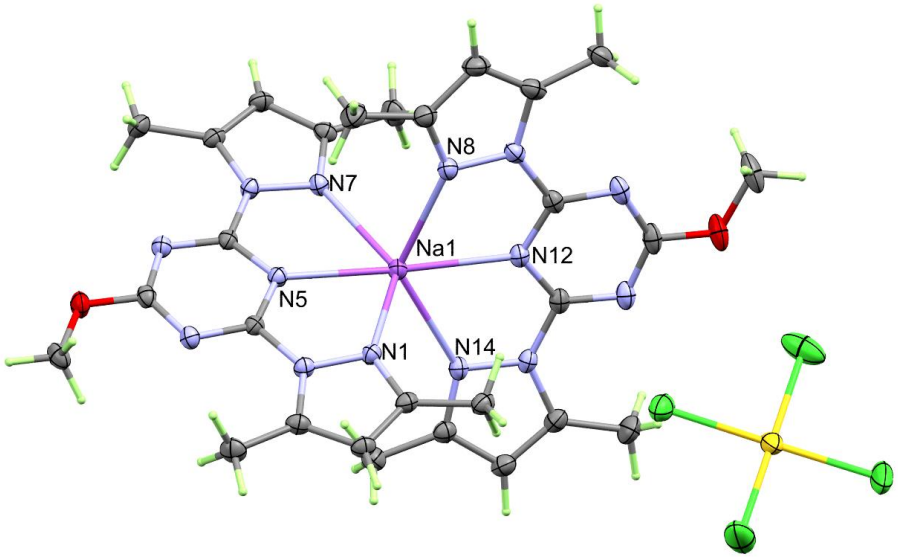

Figure 1. Structure with atom numbering for $[Na(bpmt)_2][AuCl_4]$. Atom color codes are: N: blue; O: red; C: grey; Au: yellow; Cl: green; H: light green; Na: purple.

Table 2. Bond lengths (Å) and angles (°) for $[Na(bpmt)_2][AuCl_4]$ complex.

Bond	Length/Å	Bond	Length/Å
Bond distances			
Na(1)-N(5)	2.443(3)	Na(1)-N(12)	2.429(3)
Na(1)-N(1)	2.438(3)	Na(1)-N(8)	2.469(3)
Na(1)-N(7)	2.497(3)	Na(1)-N(14)	2.538(3)
Bond angles			
N(12)-Na(1)-N(1)	112.14(9)	N(5)-Na(1)-N(7)	64.02(8)
N(12)-Na(1)-N(5)	171.65(10)	N(8)-Na(1)-N(7)	84.75(9)
N(1)-Na(1)-N(5)	64.48(8)	N(12)-Na(1)-N(14)	63.96(9)
N(12)-Na(1)-N(8)	64.98(9)	N(1)-Na(1)-N(14)	83.42(9)
N(1)-Na(1)-N(8)	108.21(9)	N(5)-Na(1)-N(14)	121.75(9)
N(5)-Na(1)-N(8)	108.19(9)	N(8)-Na(1)-N(14)	128.18(9)
N(12)-Na(1)-N(7)	118.36(9)	N(7)-Na(1)-N(14)	127.72(9)
N(1)-Na(1)-N(7)	128.40(9)		

It is worth noting that the *s*-triazine core and the two pyrazole moieties were not coplanar in the two **bpmt** ligand units. The N7N6C10C12C13 and N1N2C4C3C1 mean planes of the two pyrazole moieties formed angles of 5.32(7) and 4.81(8)°, respectively, with the N5C6N3C7N4C9 *s*-triazine core mean. The angles between the mean plane of the other *s*-triazine core N12C23N11C21N10C20 and the two pyrazole rings N13C24C26C27N14 and N9N8C15C17C18 were 11.18(9) and 8.42(8)°, respectively. Hence, the two pyrazole arms were twisted from the *s*-triazine core in both ligand units. In addition, the two **bpmt** ligand units were significantly twisted from each other, with a twist angle between their mean planes of 64.94(8)°, which significantly deviated from 90°. This deviation was possibly due to the steric preferences of the two bulky ligand units. The molecular packing of the $[Na(bpmt)_2][AuCl_4]$ complex was controlled by the important C-H···Cl and C-H···O interactions shown in Figure 2. A list of these interactions along with their corresponding geometric parameters are given in Table 3.

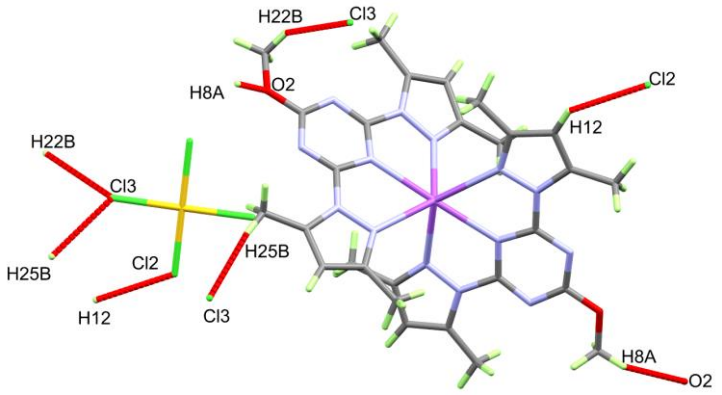

Figure 2. The important C-H···Cl and C-H···O contacts in the crystal structure of $[Na(bpmt)_2][AuCl_4]$.

Table 3. The geometric parameters of the C-H···Cl and C-H···O interactions in $[Na(bpmt)_2][AuCl_4]$ complex.

D-H···A	D-H/Å	H···A/Å	D···A/Å	D-H···A/°
C8-H8A···O2	0.98	2.470	3.214(4)	132
C12-H12···Cl2	0.95	2.948	3.776(3)	146.5
C22-H22B···Cl3	0.98	2.933	3.750(5)	141.5
C25-H25B···Cl3	0.98	2.865	3.839(4)	172.7

The molecular packing of the $[Na(bpmt)_2][AuCl_4]$ complex was controlled by three important interactions: C12-H12···Cl2, C22-H22B···Cl3, and C25-H25B···Cl3. These interactions exhibited donor to acceptor distances of 3.776(3), 3.750(5), and 3.839(4) Å, respectively. Additionally, the molecular packing was controlled by weak C8-H8A···O2 interaction. The donor C8 to acceptor O2 distance was 3.214(4) Å, while the C8-H8A···O2 angle was 132.5°. A view of the molecular packing is shown in Figure 3.

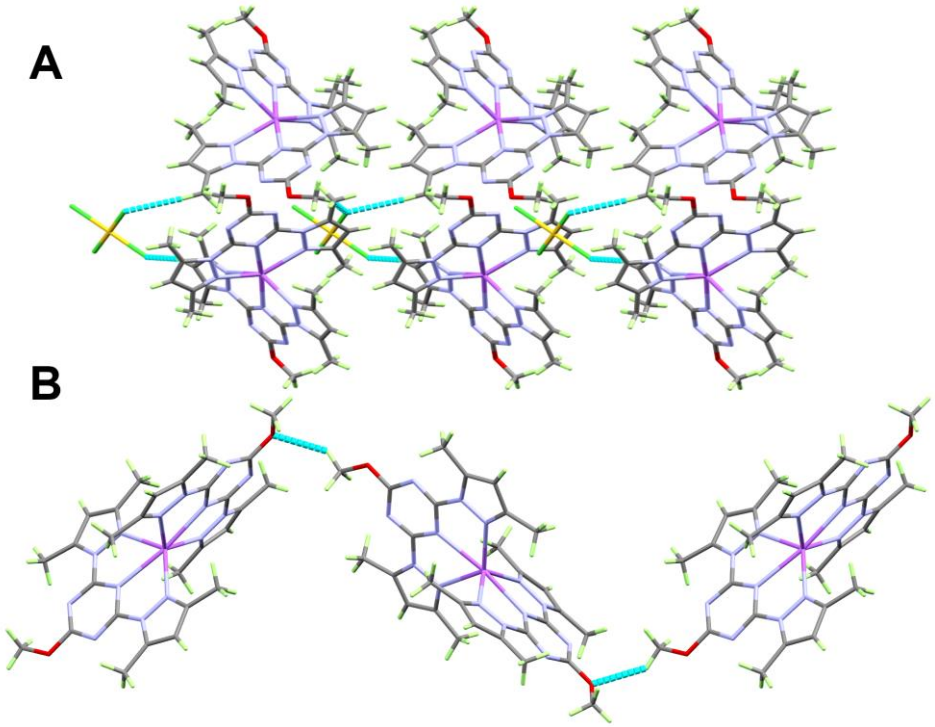

Figure 3. Packing structure for the $[Na(bpmt)_2][AuCl_4]$ complex via C-H···Cl (**A**) and C-H···O (**B**) interactions along *ac* and *bc* planes, respectively.

Furthermore, there were different levels of C-H···π interactions between H22C from the methoxy group and the pyrazole ring C24C26C27N14N13. The distance between H22C and the respective pyrazole atoms were 2.762, 2.673, 2.608, 2.665, and 2.718 Å. The H22C···centroid distance was calculated to be 2.420 Å, indicating significant C-H···π interactions. A view of the possible C-H···π interactions in the $[Na(bpmt)_2][AuCl_4]$ complex is shown in Figure 4.

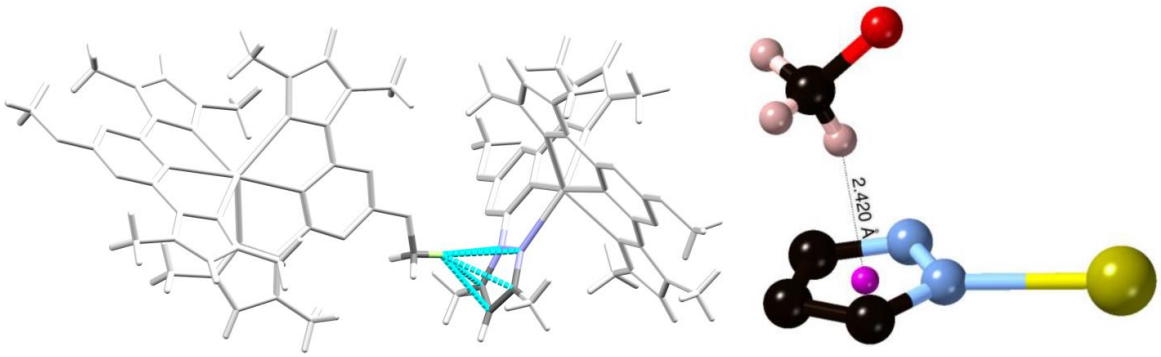

Figure 4. The possible C-H···π interactions in the $[Na(bpmt)_2][AuCl_4]$ complex.

3.3. Hirshfeld Surfaces Analyses

An analysis of the various intermolecular interactions that occurred in the crystal structure of $[Na(bpmt)_2][AuCl_4]$ was done using Hirshfeld surface calculations (Figure 5).

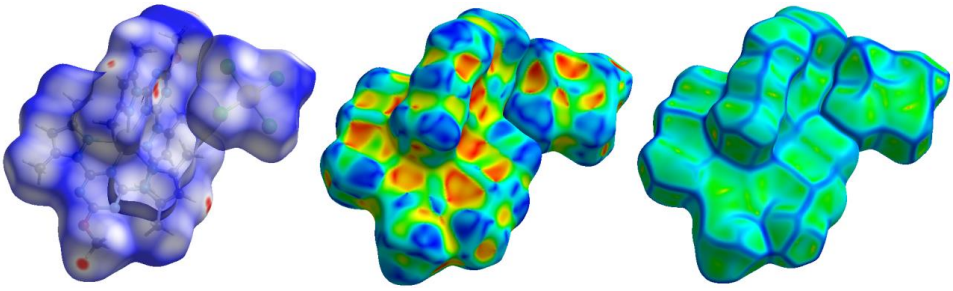

Figure 5. Hirshfeld surfaces mapped with d_{norm} (**left**), shape index (**middle**), and curvedness (**right**) for the $[Na(bpmt)_2]$ $[AuCl_4]$ complex.

In this ionic complex, the Hirshfeld analysis was performed on the cationic (A) and anionic (B) units separately. The percentages of all possible contacts in the cationic complex $[Na(bpmt)_2]^+$ (A) and anion $[AuCl_4]^-$ (B) are presented in Table 4, and are presented graphically in Figure 6.

Table 4. The percentages of all possible contacts in $[Na(bpmt)_2][AuCl_4]$ complex.

Contact	%Contact	Contact	%Contact	Contact	%Contact
	$[Na(bpmt)_2]^+$ **(A)**			$[AuCl_4]^-$ **(B)**	
Au···N	0.3	O···N	0.8	Au···O	0.1
Au···C	0.2	O···C	0.2	Au···N	1.0
Au···H	0.5	O···H	4.9	Au···C	0.6
Cl···O	0.8	N···N	0.5	Au···H	5.7
Cl···N	2.0	N···C	0.6	Cl···O	3.7
Cl···C	1.9	N···H	9.3	Cl···N	7.6
Cl···H	12.2	C···C	0.6	Cl···C	7.1
Na···O	0.1	C···H	11.5	Cl···H	74.1
Na···H	0.2	H···H	53.4		

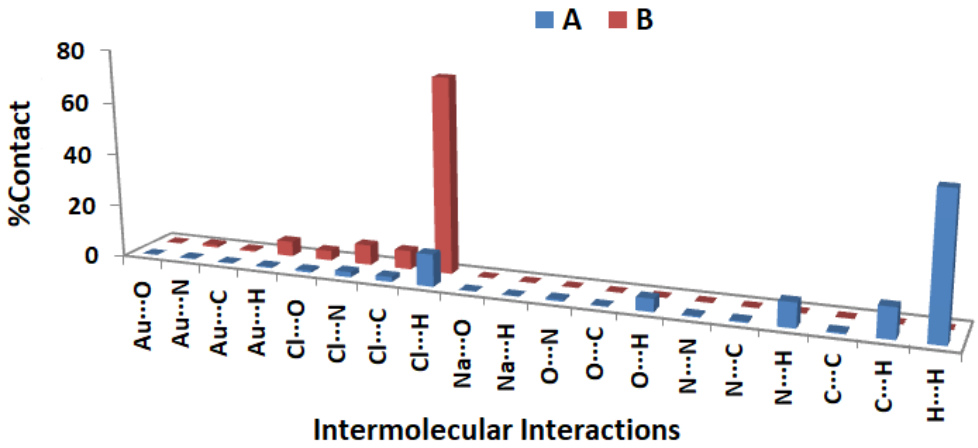

Figure 6. All of the possible intermolecular contacts in the $[Na(bpmt)_2][AuCl_4]$ complex. A and B refer to the cationic and anionic parts of the $[Na(bpmt)_2][AuCl_4]$ complex, respectively.

The Hirshfeld surfaces of the $[Na(bpmt)_2][AuCl_4]$ complex, mapped with d_{norm}, shape index, and curvedness, are shown in Figure 5. Short contacts are apparent as deep red areas, while the white areas are related to contacts near the van der Waals radii sum

of the interacting atoms, which were considered the most important in the molecular packing. Conversely, the blue areas represent long-distance interactions. The bright red spots on the d_{norm} maps represent the areas where H···H, Cl···H, C···H, N···H, and O···H interactions occurred. The decomposition of the fingerprint plot indicates their percentages in the cationic $[Na(bpmt)_2]^+$ (A) unit were 53.4, 12.2, 11.5, 9.3, and 4.9%, respectively. These contacts also appeared as sharp spikes in the fingerprint plots (Figure 7). The other intermolecular contacts, which appeared as blue areas in the d_{norm} maps, were less significant, and their intermolecular contacts were typically weak. The absence of red/blue triangles in the shape index map revealed that no aromatic π-π stacking contacts were present. Furthermore, the curved green regions in the curvedness map confirmed the absence of π-π stacking interactions.

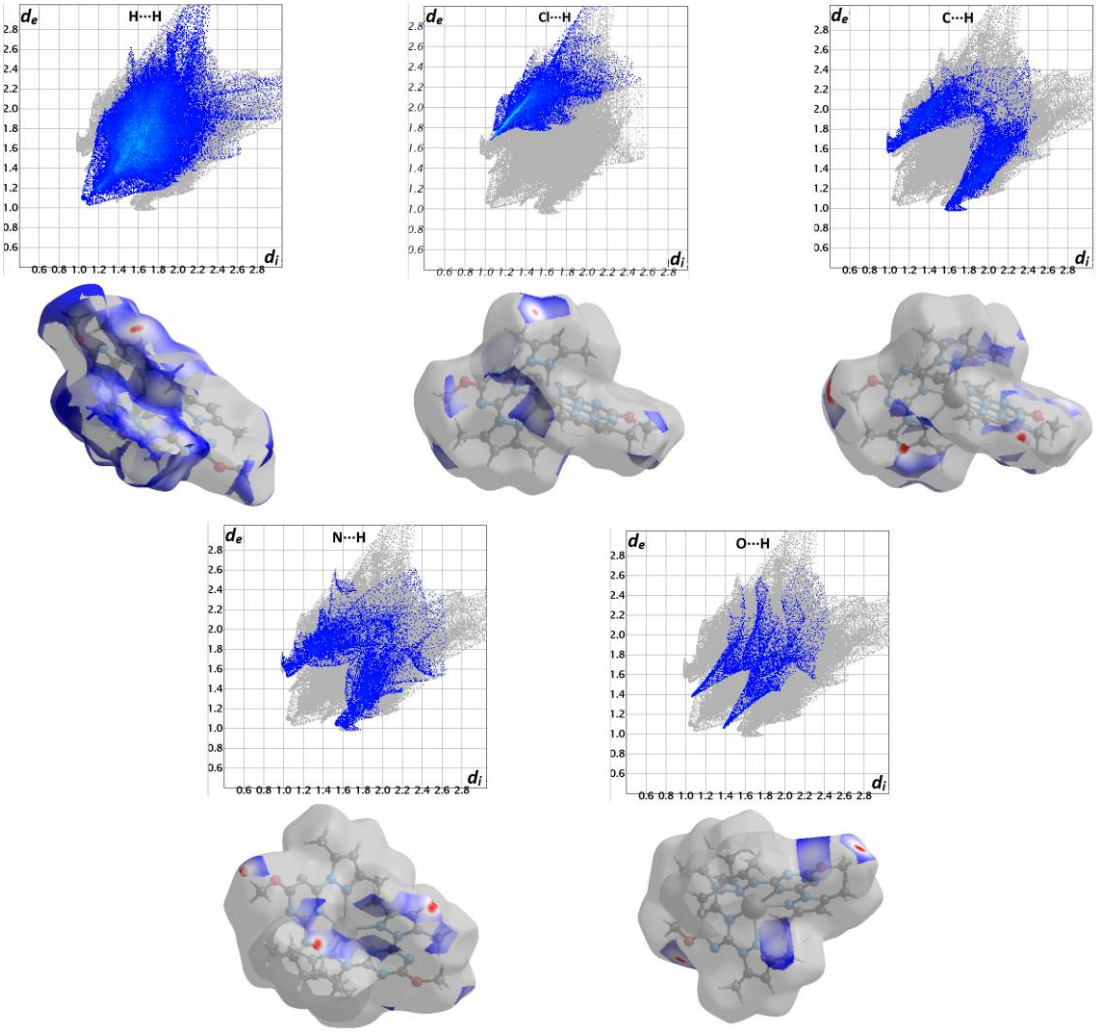

Figure 7. The d_{norm} maps and fingerprint plots of the most important interactions in the cationic complex unit $[[Na(bpmt)_2]^+$ (A).

For the anionic unit $[AuCl_4]^-$ (B), the significant contact observed was the Cl···H interaction, while other contacts had less significance. In this unit, the percentage of the Cl···H contacts was 74.1%. This type of non-covalent interaction exhibits the characteristics of short interactions, as clearly depicted in Figure 8.

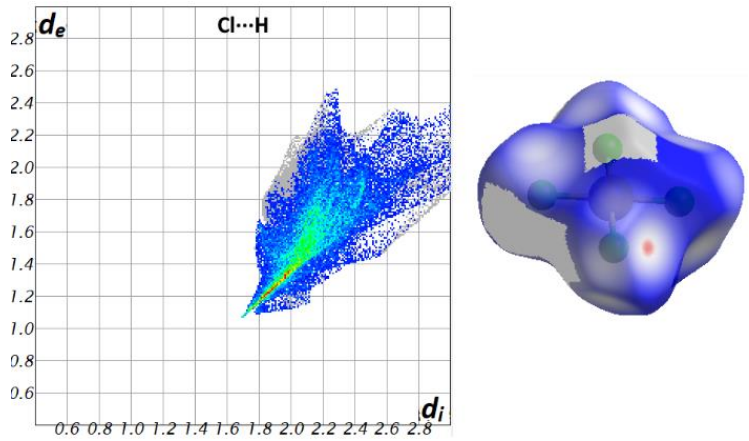

Figure 8. The d_{norm} map and fingerprint plot of Cl···H contact in the $[AuCl_4]^-$ anion.

3.4. Antimicrobial Studies

The antimicrobial activity of the free **bpmt** and its $[Na(bpmt)_2][AuCl_4]$ pincer complex against a number of specified pathogenic microorganisms was evaluated. The minimum concentration that showed no observable microbial growth was determined as the minimum inhibitory concentration (MIC), and the results are listed in Table 5. The MIC data demonstrated that the free **bpmt** had no antibacterial activity against any of the studied strains except for *K. pneumonia* (50) and *A. baumannii* (8). On the other hand, the $[Na(bpmt)_2][AuCl_4]$ complex showed improved antimicrobial activity against most bacterial strains compared to **bpmt**. The only exceptions were *K. pneumonia* (50), *K. pneumonia* (R124), and *A. baumannii* (8), where both compounds exhibited similar actions. The corresponding MIC values were 62.5, 500, and 125 μg/mL, respectively.

Table 5. MIC values (μg/mL) of the $[Na(bpmt)_2][AuCl_4]$ complex and its free ligand **bpmt**.

Tested Compound	bpmt	$[Na(bpmt)_2][AuCl_4]$	Control
Gram-positive bacteria			
S. aureus (ATCC 25923)	500	125	≤7.8 [a]
MRSA (ATCC43300)	500	125	>500 [a]
MRSA (1)	500	125	>500 [a]
E. fecium (31)	500	125	>500 [a]
Gram-negative bacteria			
E. coli (ATCC 25922)	500	125	62.5 [a]
K. pneumonia (ATCC 700603)	500	125	>500 [a]
P. aeruginosa (ATCC 29853)	500	125	125 [a]
A. baumannii (ATCC 19606)	500	125	>500 [a]
P. miabilis	500	125	125 [a]
K. pneumonia (50)	62.5	62.5	>500 [a]
K. pneumonia isolates (R124)	500	500	>500 [a]
P. aeruginosa (5)	500	125	500 [a]
A. baumannii (8)	125	125	>500 [a]
Fungi			
C. albicans	500	125	15.6 [b]

[a] Amoxicillin; [b] Nystatin.

Interestingly, the MIC values of the $[Na(bpmt)_2][AuCl_4]$ complex were in the range of 62.5–125 μg/mL, indicating higher antibacterial activity against most of the investigated bacteria compared to Amoxicillin (MIC > 500) as a standard antibiotic. It is clear that the $[Na(bpmt)_2][AuCl_4]$ complex had higher MIC values (125 μg/mL) than Amoxicillin only for *S. aureus* and *E. coli* (≤7.8 and 62.5 μg/mL, respectively), and exhibited

similar MIC values to Amoxicillin for *P. aeruginosa*, *P. miabilis*, and *K. pneumonia* (R124) (125, 125, and 500 µg/mL, respectively). In contrast, the free ligand **bpmt** demonstrated good antibacterial activity against only two bacterial strains, *K. pneumonia* (50) and *A. baumannii* (8), with MIC values of 62.5 and 125 µg/mL, respectively, compared to Amoxicillin (MIC > 500).

The $[Na(bpmt)_2][AuCl_4]$ complex exhibited better antifungal activity than the free ligand **bpmt**. The MIC values were determined to be 125 and 500 µg/mL, respectively. Compared with Nystatin (MIC = 15.6 µg/mL), a standard antifungal medication, the $[Na(bpmt)_2][AuCl_4]$ complex and its free **bpmt** ligand had lower antifungal activity against the studied fungus, *C. albicans*. Thus, the results revealed that the $[Na(bpmt)_2][AuCl_4]$ complex had significant antibacterial properties against most of the gram-positive and gram-negative bacteria. Additionally, the $[Na(bpmt)_2][AuCl_4]$ complex showed promising antifungal activity against *C. albicans* when compared to **bpmt.**

4. Conclusions

The novel $[Na(bpmt)_2][AuCl_4]$ complex was obtained as highly crystalline product by reacting the **bpmt** pincer ligand with $Na[AuCl_4].2H_2O$ using the self-assembly technique. Its structure was analyzed using single crystal X-ray diffraction, FTIR, and NMR spectroscopic techniques, in addition to elemental analysis and Hirshfeld topology analysis. The mononuclear homoleptic $[Na(bpmt)_2][AuCl_4]$ complex had hexa-coordinated Na(I) with a distorted octahedral geometry. Hirshfeld studies were used to explore the importance of the H···H, Cl···H, C···H, N···H, and O···H contacts in the supramolecular structure of the $[Na(bpmt)_2][AuCl_4]$ complex. Antimicrobial evaluation of the studied Na(I) complex revealed promising antibacterial and antifungal activities compared to the free **bpmt** ligand.

Supplementary Materials: The following supporting information can be downloaded at: https://www.mdpi.com/article/10.3390/cryst13060890/s1, Figure S1: FTIR spectra of the free ligand **bpmt**; Figure S2: FTIR spectra of the $[Na(bpmt)_2][AuCl_4]$ complex; Figure S3: ^1H and ^{13}C NMR spectra of the free ligand (**bpmt**); Figure S4: ^1H and ^{13}C NMR spectra of $[Na(bpmt)_2][AuCl_4]$; Method S1: Antimicrobial activity assay.

Author Contributions: Conceptualization, S.M.S., M.S.A., M.A.M.A.-Y. and L.Ö.; methodology, A.Y.; software, S.M.S., M.H. and L.Ö.; validation, M.M.F.I., N.G.E.M., M.H. and L.Ö.; formal analysis, A.Y., M.M.F.I. and N.G.E.M.; investigation, A.Y., A.E.-F. and M.S.A.; resources, A.E.-F., M.A.M.A.-Y. and A.B.; data curation, L.Ö. and A.Y.; writing—original draft preparation, A.Y., A.E.-F., S.M.S., M.H., M.M.F.I., N.G.E.M. and L.Ö.; writing—review and editing, A.Y., M.A.M.A.-Y., S.M.S., M.S.A., M.M.F.I., N.G.E.M. and L.Ö.; visualization, A.Y., S.M.S. and L.Ö.; supervision, M.A.M.A.-Y., M.S.A., S.M.S. and L.Ö.; project administration, M.A.M.A.-Y. and A.B.; funding acquisition, A.B. All authors have read and agreed to the published version of the manuscript.

Funding: The authors would like to extend their sincere appreciation to the Researchers Supporting Project (RSP2023R64), King Saud University, Riyadh, Saudi Arabia.

Data Availability Statement: Not applicable.

Acknowledgments: The authors would like to extend their sincere appreciation to the Researchers Supporting Project (RSP2023R64), King Saud University, Riyadh, Saudi Arabia.

Conflicts of Interest: The authors declare no conflict of interest.

References

1. Chu, D.T.; Plattner, J.J.; Katz, L. New directions in antibacterial research. *J. Med. Chem.* **1996**, *39*, 3853–3874. [CrossRef] [PubMed]
2. Evans, A.; Kavanagh, K.A. Evaluation of metal-based antimicrobial compounds for the treatment of bacterial pathogens. *Int. J. Med. Microbiol.* **2021**, *70*, 001363. [CrossRef] [PubMed]
3. Dalla Via, L.; Marciani Magno, S.; Gia, O.; Marini, A.M.; Da Settimo, F.; Salerno, S.; La Motta, C.; Simorini, F.; Taliani, S.; Lavecchia, A. Benzothiopyranoindole-based antiproliferative agents: Synthesis, cytotoxicity, nucleic acids interaction, and topoisomerases inhibition properties. *J. Med. Chem.* **2009**, *52*, 5429–5441. [CrossRef] [PubMed]

4. Soliman, S.M.; El-Faham, A.; El Silk, S.E. Novel one-dimensional polymeric Cu(II) complexes via Cu(II)-assisted hydrolysis of the 2,4-*bis*(3,5-dimethyl-1*H*-pyrazol-1-yl)-6-methoxy-1,3,5-triazine pincer ligand: Synthesis, structure, and antimicrobial activities. *Appl. Organomet. Chem.* **2020**, *34*, e5941. [CrossRef]
5. Fujimoto, S.; Yasui, H.; Yoshikawa, Y. Development of a novel antidiabetic zinc complex with an organoselenium ligand at the lowest dosage in KK-A^{y} mice. *J. Inorg. Biochem.* **2013**, *121*, 10–15. [CrossRef]
6. Huang, Q.; Pan, Z.; Wang, P.; Chen, Z.; Zhang, X.; Xu, H. Zinc(II) and copper(II) complexes of β-substituted hydroxylporphyrins as tumor photosensitizers. *Bioorg. Med. Chem. Lett.* **2006**, *16*, 3030–3033. [CrossRef]
7. Paesa, M.; de Ganuza, C.R.; Alejo, T.; Yus, C.; Irusta, S.; Arruebo, M.; Sebastian, V.; Mendoza, G. Elucidating the mechanisms of action of antibiotic-like ionic gold and biogenic gold nanoparticles against bacteria. *J. Colloid Interface Sci.* **2023**, *633*, 786–799. [CrossRef]
8. Blake, A.J.; Champness, N.R.; Hubberstey, P.; Li, W.-S.; Withersby, M.A.; Schröder, M. Inorganic crystal engineering using self-assembly of tailored building-blocks. *Coord. Chem. Rev.* **1999**, *183*, 117–138. [CrossRef]
9. Braga, D.; Maini, L.; Polito, M.; Scaccianoce, L.; Cojazzi, G.; Grepioni, F. Design of organometallic molecular and ionic materials. *Coord. Chem. Rev.* **2001**, *216*, 225–248. [CrossRef]
10. Moulton, B.; Zaworotko, M.J. From molecules to crystal engineering: Supramolecular isomerism and polymorphism in network solids. *Chem. Rev.* **2001**, *101*, 1629–1658. [CrossRef]
11. McManus, G.J.; Perry, J.J., IV; Perry, M.; Wagner, B.D.; Zaworotko, M.J. Exciplex fluorescence as a diagnostic probe of structure in coordination polymers of Zn^{2+} and 4,4′-bipyridine containing intercalated pyrene and enclathrated aromatic solvent guests. *J. Am. Chem. Soc.* **2007**, *129*, 9094–9101. [CrossRef]
12. Macgillivray, L.R.; Papaefstathiou, G.S.; Friščić, T.; Hamilton, T.D.; Bučar, D.-K.; Chu, Q.; Varshney, D.B.; Georgiev, I.G. Supramolecular control of reactivity in the solid state: From templates to ladderanes to metal−organic frameworks. *Acc. Chem. Res.* **2008**, *41*, 280–291. [CrossRef]
13. Verbalis, J.G. Disorders of body water homeostasis. *Best Pract. Res. Clin. Endocrinol. Metab.* **2003**, *17*, 471–503. [CrossRef]
14. Fraser, S.P.; Ozerlat-Gunduz, I.; Brackenbury, W.J.; Fitzgerald, E.M.; Campbell, T.M.; Coombes, R.C.; Djamgoz, M.B. Regulation of voltage-gated sodium channel expression in cancer: Hormones, growth factors and auto-regulation. *Philos. Trans. R. Soc. Lond. B Biol. Sci.* **2014**, *369*, 20130105. [CrossRef]
15. Li, M.; Xiong, Z.-G. Ion channels as targets for cancer therapy. *Int. J. Physiol. Pathophysiol. Pharmacol.* **2011**, *3*, 156–166.
16. Arcangeli, A.; Crociani, O.; Lastraioli, E.; Masi, A.; Pillozzi, S.; Becchetti, A. Targeting ion channels in cancer: A novel frontier in antineoplastic therapy. *Curr. Med. Chem.* **2009**, *16*, 66–93. [CrossRef]
17. Prevarskaya, N.; Skryma, R.; Shuba, Y. Ion channels and the hallmarks of cancer. *Trends Mol. Med.* **2010**, *16*, 107–121. [CrossRef]
18. McCarthy, J.V.; Cotter, T.G. Cell shrinkage and apoptosis: A role for potassium and sodium ion efflux. *Cell Death Differ.* **1997**, *4*, 756–770. [CrossRef]
19. Temel, H.; Hoşgören, H.; Çakır, Ü.; Boybay, M. Synthesis and Characterization of Na^{+} and Ba^{2+} Complexes with Some Lipophilic Diaza-18-Crown-6 Derivatives. In Proceedings of the Ninth International Symposium on Molecular Recognition and Inclusion, Lyon, France, 7–12 September 1996; Coleman, A.W., Ed.; Springer: Berlin/Heidelberg, Germany, 1998; pp. 527–530.
20. Dou, J.; Li, D.; Sun, D.; Liu, Y.; Xu, L.; Bi, W.; Zheng, P. One-dimensional chain crown ether complex synthesis and crystal structure of novel complex:{[Na(18C6)][Na(18C6)(H_2O)]}[Cu(mnt)$_2$]. *Indian J. Chem.* **2001**, *40A*, 878–879.
21. Xi-Shi, T.; Guang-Li, W.; Yuan-Yuan, L. Synthesis and crystal structure of a Na(I) complex with 4,4′-bipyridine and 2-formylbenzenesulfonate-hydrazine. *St. Cerc. St. CICBIA* **2015**, *16*, 173–177.
22. Wang, L.H.; Ji, Z.X. Crystal structure of Na(I) complex with 1,5-naphthalenedisulfonate. In *Advanced Materials Research*; Trans Tech Publications Ltd.: Zurich, Switzerland, 2014; pp. 185–188.
23. Jia, R.; Gao, T.; Chen, R.; Yang, Y.; Gao, P.; Wang, Y.; Yan, P. Syntheses and structures of homodinuclear (Na–Na) and heterodinuclear (Cu–Na, Cu–K) metal complexes. *Aust. J. Chem.* **2015**, *69*, 20–26. [CrossRef]
24. Li, N.; Wang, M.; Ma, C.-B.; Hu, M.-Q.; Zhou, R.-W.; Chen, H.; Chen, C.-N. Synthesis and characterization of a new 2D trimetallic Mn/Ca/Na complex. *Inorg. Chem. Commun.* **2010**, *13*, 730–732. [CrossRef]
25. Wang, R.-M.; Duan, Z.-F.; He, Y.-F.; Lei, Z.-Q. Heterogeneous catalytic aerobic oxidation behavior of Co–Na heterodinuclear polymeric complex of salen-crown ether. *J. Mol. Catal.* **2006**, *260*, 280–287. [CrossRef]
26. Liu, X.; Xie, C.; Wang, X.; Shen, G.; Shen, D. A novel 2D polymeric structure of Cu–Na complex, in which phthalate gives seven coordination sites. *Inorg. Chem. Commun.* **2003**, *6*, 1433–1435. [CrossRef]
27. Hogerheide, M.P.; Ringelberg, S.N.; Janssen, M.D.; Boersma, J.; Spek, A.L.; van Koten, G. Influence of intramolecular coordination on the aggregation of sodium phenolate complexes. X-ray structures of [$NaOC_6H_4(CH_2NMe_2)$-2]$_6$ and [$Na(OC_6H_2(CH_2NMe_2)_2$-2,6-Me-4)($HOC_6H_2(CH_2NMe_2)_2$-2,6-Me-4)]$_2$. *Inorg. Chem.* **1996**, *35*, 1195–1200. [CrossRef]
28. Wang, H.-S.; Zhang, K.; Wang, J.; Hu, Z.; Song, Y.; Zhang, Z.; Pan, Z.-Q. Regulating the distortion degree of the square antiprism coordination geometry in Dy–Na single ion magnets. *CrystEngComm* **2021**, *23*, 3175–3184. [CrossRef]
29. Xu, X.; Ma, M.; Yao, Y.; Zhang, Y.; Shen, Q. Synthesis, characterisation of carbon-bridged (diphenolato) lanthanide complexes and their catalytic activity for diels–alder reactions. *Eur. J. Inorg. Chem.* **2005**, *2005*, 676–684. [CrossRef]
30. Cunningham, D.; McArdle, P.; Mitchell, M.; Ní Chonchubhair, N.; O'Gara, M.; Franceschi, F.; Floriani, C. Adduct formation between alkali metal ions and divalent metal salicylaldimine complexes having methoxy substituents. A structural investigation. *Inorg. Chem.* **2000**, *39*, 1639–1649. [CrossRef]

31. Goudarzi, A.; Saeidifar, M.; Aghapoor, K.; Mohsenzadeh, F.; Fenske, D.; Fuhr, O.; Ghassemzadeh, M. Unprecedented bi-and trinuclear palladium(II)-sodium complexes from a salophen-type schiff base: Synthesis, characterization, thermal behavior, and in vitro biological activities. *J. Mol. Struct.* **2023**, *1272*, 134224. [CrossRef]
32. Wani, M.Y.; Silva, M.R.; Krishnakumar, B.; Kumar, S.; Al-Bogami, A.S.; Aqlan, F.M.; Sobral, A.J. Catalytic synthesis of 5-substituted tetrazoles: Unexpected reactions and products. *J. Heterocycl. Chem.* **2019**, *56*, 1613–1621. [CrossRef]
33. Belveren, S.; Poyraz, S.; Ülger, M.; Pask, C.M.; Döndaş, H.A.; Sansano, J.M. Synthesis, structure and bioactivity of a mononuclear octahedral [prolinate$_2$-Na(MeOH)$_4$]$^-$ H$^+$ complex. *Inorganica Chim. Acta* **2020**, *504*, 119456. [CrossRef]
34. Laid, P.; Gourdon, A.; Launay, J.-P. Chemistry of Iron with Dipicolinic Acid. 1. Mononuclear Complexes of Iron(I1) or Iron(1II). *Inorg. Chem.* **1995**, *34*, 5129–5137.
35. Brown, A.; Bunchuay, T.; Crane, C.G.; White, N.G.; Thompson, A.L.; Beer, P.D. A Bis-Triazacyclononane Tris-Pyridyl N9-Azacryptand "Beer Can" Receptor for Complexation of Alkali Metal and Lead(II) Cations. *Chem. Eur. J.* **2018**, *24*, 10434–10442. [CrossRef] [PubMed]
36. Jeon, Y.-M.; Kim, J.; Whang, D.; Kim, K. Molecular container assembly capable of controlling binding and release of its guest molecules: Reversible encapsulation of organic molecules in sodium ion complexed cucurbituril. *J. Am. Chem. Soc.* **1996**, *118*, 9790–9791. [CrossRef]
37. Piotrowski, H.; Polborn, K.; Hilt, G.; Severin, K. A self-assembled metallomacrocyclic ionophore with high affinity and selectivity for Li$^+$ and Na$^+$. *J. Am. Chem. Soc.* **2001**, *123*, 2699–2700. [CrossRef] [PubMed]
38. Khristolyubov, D.O.; Lyubov, D.M.; Cherkasov, A.V.; Fukin, G.K.; Shavyrin, A.S.; Trifonov, A.A. Alkali-metal alkyl complexes with the tridentate benzhydryl ligand [2,2′-(4-MeC$_6$H$_4$NMe$_2$)$_2$CH]$^-$. *Organometallics* **2018**, *37*, 1627–1634. [CrossRef]
39. Menicagli, R.; Samaritani, S.; Signore, G.; Vaglini, F.; Dalla Via, L. In vitro cytotoxic activities of 2-alkyl-4,6-diheteroalkyl-1,3,5-triazines: New molecules in anticancer research. *J. Med. Chem.* **2004**, *47*, 4649–4652. [CrossRef]
40. Pandey, V.K.; Tusi, S.; Tusi, Z.; Joshi, M.; Bajpai, S. Synthesis and biological activity of substituted 2,4,6-s-triazines. *Acta Pharm.* **2004**, *54*, 1–12.
41. Lübbers, T.; Angehrn, P.; Gmünder, H.; Herzig, S.; Kulhanek, J. Design, synthesis, and structure–activity relationship studies of ATP analogues as DNA gyrase inhibitors. *Bioorg. Med. Chem. Lett.* **2000**, *10*, 821–826. [CrossRef]
42. Al-Khodir, F.A.; Al-Warhi, T.; Abumelha, H.M.; Al-Issa, S. Synthesis, chemical and biological investigations of new Ru(III) and Se(IV) complexes containing 1,3,5-triazine chelating derivatives. *J. Mol. Struct.* **2019**, *1179*, 795–808. [CrossRef]
43. Klenke, B.; Stewart, M.; Barrett, M.P.; Brun, R.; Gilbert, I.H. Synthesis and biological evaluation of s-triazine substituted polyamines as potential new anti-trypanosomal drugs. *J. Med. Chem.* **2001**, *44*, 3440–3452. [CrossRef]
44. Fadaly, W.A.; Elshaier, Y.A.; Nemr, M.T.; Abdellatif, K.R. Design, synthesis, modeling studies and biological evaluation of pyrazole derivatives linked to oxime and nitrate moieties as nitric oxide donor selective COX-2 and aromatase inhibitors with dual anti-inflammatory and anti-neoplastic activities. *Bioorg. Chem.* **2023**, *134*, 106428. [CrossRef]
45. Rabah, R.R.A.; Sebastian, A.; Vunnam, S.; Sultan, S.; Tarazi, H.; Anbar, H.S.; Shehata, M.K.; Zaraei, S.-O.; Elgendy, S.M.; Al Shamma, S.A. Design, synthesis, and biological evaluation of a new series of pyrazole derivatives: Discovery of potent and selective JNK3 kinase inhibitors. *Bioorg. Med. Chem.* **2022**, *69*, 116894. [CrossRef]
46. Ali, S.A.; Awad, S.M.; Said, A.M.; Mahgoub, S.; Taha, H.; Ahmed, N.M. Design, synthesis, molecular modelling and biological evaluation of novel 3-(2-naphthyl)-1-phenyl-1H-pyrazole derivatives as potent antioxidants and 15-lipoxygenase inhibitors. *J. Enzyme Inhib. Med. Chem.* **2020**, *35*, 847–863. [CrossRef]
47. Dahlous, K.A.; Soliman, S.M.; El-Faham, A.; Massoud, R.A. Synthesis, molecular and supramolecular structures of symmetric dinuclear Cd(II) azido complex with *bis*-pyrazolyl *s*-triazine pincer ligand. *Symmetry* **2022**, *14*, 2409. [CrossRef]
48. Soliman, S.M.; Almarhoon, Z.; Sholkamy, E.N.; El-Faham, A. *Bis*-pyrazolyl-*s*-triazine Ni(II) pincer complexes as selective gram positive antibacterial agents; synthesis, structural and antimicrobial studies. *J. Mol. Struct.* **2019**, *1195*, 315–322. [CrossRef]
49. Soliman, S.M.; Almarhoon, Z.; El-Faham, A. Synthesis, molecular and supramolecular structures of new Cd(II) pincer-type complexes with *s*-triazine core ligand. *Crystals* **2019**, *9*, 226. [CrossRef]
50. Soliman, S.M.; El-Faham, A. Synthesis, X-ray structure, and DFT studies of five-and eight-coordinated Cd(II) complexes with *s*-triazine *N*-pincer chelate. *J. Coord. Chem.* **2019**, *72*, 1621–1636. [CrossRef]
51. Refaat, H.M.; Alotaibi, A.A.; Dege, N.; El-Faham, A.; Soliman, S.M. Synthesis, structure and biological evaluations of Zn(II) pincer complexes based on *s*-triazine type chelator. *Molecules* **2022**, *27*, 3625. [CrossRef]
52. Refaat, H.M.; Alotaibi, A.A.; Dege, N.; El-Faham, A.; Soliman, S.M. Co(II) complexes based on the *bis*-pyrazol-*s*-triazine pincer ligand: Synthesis, X-ray structure studies, and cytotoxic evaluation. *Crystals* **2022**, *12*, 741–750. [CrossRef]
53. Soliman, S.M.; Elsilk, S.E.; El-Faham, A. Syntheses, structure, Hirshfeld analysis and antimicrobial activity of four new Co(II) complexes with *s*-triazine-based pincer ligand. *Inorg. Chim. Acta* **2020**, *510*, 119753. [CrossRef]
54. Dahlous, K.A.; Soliman, S.M.; El-Faham, A.; Massoud, R.A. Synthesis and X-ray structure combined with Hirshfeld and aim studies on a new trinuclear Zn(II)-azido complex with *s*-triazine pincer ligand. *Crystals* **2022**, *12*, 1786–1799. [CrossRef]
55. Lasri, J.; Al-Rasheed, H.H.; El-Faham, A.; Haukka, M.; Abutaha, N.; Soliman, S.M. Synthesis, structure and in vitro anticancer activity of Pd(II) complexes of mono-and *bis*-pyrazolyl-*s*-triazine ligands. *Polyhedron* **2020**, *187*, 114665. [CrossRef]
56. Soliman, S.M.; Elsilk, S.E.; El-Faham, A. Synthesis, structure and biological activity of Zinc(II) pincer complexes with 2,4-*bis*(3,5-dimethyl-1*H*-pyrazol-1-yl)-6-methoxy-1,3,5-triazine. *Inorg. Chim. Acta* **2020**, *508*, 119627. [CrossRef]

57. Soliman, S.M.; El-Faham, A. Synthesis, characterization, and structural studies of two heteroleptic Mn(II) complexes with tridentate *N*,*N*,*N*-pincer type ligand. *J. Coord. Chem.* **2018**, *71*, 2373–2388. [CrossRef]
58. Soliman, S.M.; Massoud, R.A.; Al-Rasheed, H.H.; El-Faham, A. Syntheses and structural investigations of penta-coordinated Co(II) complexes with *bis*-pyrazolo-*s*-triazine pincer ligands, and evaluation of their antimicrobial and antioxidant activities. *Molecules* **2021**, *26*, 3633. [CrossRef]
59. Soliman, S.M.; El-Faham, A. One pot synthesis of two Mn(II) perchlorate complexes with *s*-triazine *NNN*-pincer ligand; molecular structure, Hirshfeld analysis and DFT studies. *J. Mol. Struct.* **2018**, *1164*, 344–353. [CrossRef]
60. Otwinowski, Z.; Minor, W. Processing of X-ray Diffraction Data Collected in Oscillation Mode. *Methods Enzymol.* **1997**, *276*, 307–326.
61. Sheldrick, G.M. *SADABS-Bruker Nonius Scaling and Absorption Correction*; Bruker AXS, Inc.: Madison, WI, USA, 2012.
62. Sheldrick, G.M. Shelxt–integrated space-group and crystal-structure determination. *Acta Cryst.* **2015**, *A71*, 3–8. [CrossRef]
63. Sheldrick, G.M. Crystal structure refinement with SHELXL. *Acta Cryst.* **2015**, *C71*, 3–8.
64. Hübschle, C.B.; Sheldrick, G.M.; Dittrich, B. A Qt Graphical User Interface for SHELXL. *J. Appl. Cryst.* **2011**, *44*, 1281–1284. [CrossRef]
65. Mackenzie, C.F.; Spackman, P.R.; Jayatilaka, D.; Spackman, M.A. Crystalexplorer model energies and energy frameworks: Extension to metal coordination compounds, organic salts, solvates and open-shell systems. *IUCrJ* **2017**, *4*, 575–587. [CrossRef]
66. Hirshfeld, F.L. Bonded-atom fragments for describing molecular charge densities. *Theor. Chim. Acta* **1977**, *44*, 129–138. [CrossRef]
67. Wayne, P. Clinical and laboratory standards institute: Performance standards for antimicrobial susceptibility testing: 20th informational supplement. In *CLSI Document M100-S20*; Clinical and Laboratory Standards Institute: Wayne, NY, USA, 2010.